

ARTICLE

Received 1 Oct 2015 | Accepted 18 Feb 2016 | Published 7 Apr 2016

DOI: 10.1038/ncomms11090

OPEN

Light-enhanced liquid-phase exfoliation and current photoswitching in graphene-azobenzene composites

Markus Döbbelin¹, Artur Ciesielski¹, Sébastien Haar¹, Silvio Osella², Matteo Bruna³, Andrea Minoia², Luca Grisanti², Thomas Mosciatti¹, Fanny Richard¹, Eko Adi Prasetyanto⁴, Luisa De Cola⁴, Vincenzo Palermo⁵, Raffaello Mazzaro^{6,7}, Vittorio Morandi⁶, Roberto Lazzaroni², Andrea C. Ferrari³, David Beljonne² & Paolo Samori¹

Multifunctional materials can be engineered by combining multiple chemical components, each conferring a well-defined function to the ensemble. Graphene is at the centre of an ever-growing research effort due to its combination of unique properties. Here we show that the large conformational change associated with the *trans-cis* photochemical isomerization of alkyl-substituted azobenzenes can be used to improve the efficiency of liquid-phase exfoliation of graphite, with the photochromic molecules acting as dispersion-stabilizing agents. We also demonstrate reversible photo-modulated current in two-terminal devices based on graphene-azobenzene composites. We assign this tuneable electrical characteristics to the intercalation of the azobenzene between adjacent graphene layers and the resulting increase in the interlayer distance on (photo)switching from the linear *trans*-form to the bulky *cis*-form of the photochromes. These findings pave the way to the development of new optically controlled memories for light-assisted programming and high-sensitive photosensors.

¹Nanochemistry Laboratory, ISIS & icFRC, Université de Strasbourg & CNRS, 8 allée Gaspard Monge, 67000 Strasbourg, France. ²Laboratory for Chemistry of Novel Materials, University of Mons, Place du Parc 20, B-7000 Mons, Belgium. ³Cambridge Graphene Centre, University of Cambridge, 9 JJ Thomson Avenue, Cambridge CB3 0FA, UK. ⁴Laboratory of Supramolecular Biomaterials and Chemistry, ISIS & icFRC, Université de Strasbourg & CNRS, 8 allée Gaspard Monge, 67000 Strasbourg, France. ⁵ISOF-CNR, via Gobetti 101, 40129 Bologna, Italy. ⁶IMM-CNR Sezione di Bologna, via Gobetti, 101, 40129 Bologna, Italy. ⁷Dipartimento di Chimica 'G. Ciamician', Università di Bologna, via Selmi 2, 40126 Bologna, Italy. Correspondence and requests for materials should be addressed to A.C. (email:ciesielski@unistra.fr) or to P.S. (email:samori@unistra.fr).

Graphene is a one-atom-thick two-dimensional material with unique mechanical, optical, thermal and electrical properties¹, promising future emerging technologies, including flexible and wearable electronics². Two main approaches are being followed for graphene production: bottom-up and top-down³. The former relies on the assembly of suitably designed molecular building blocks, undergoing chemical reaction to form covalently linked networks⁴. The latter occurs via exfoliation of graphite into graphene^{3,5}. Bottom-up techniques, in particular those based on organic syntheses starting from small molecular modules^{6,7}, when performed in liquid media, are both size limited, because macromolecules become less soluble with increasing size⁶, and suffer from the occurrence of side reactions with increasing molecular weight⁶. The growth on solid (ideally catalytically active) surfaces allows one to circumvent these issues. Substrate-based growth can also be achieved by chemical vapour deposition (CVD)^{8,9} or via silicon evaporation from silicon carbide¹⁰, which rely on the ability to follow a narrow thermodynamic path. Top-down approaches can be accomplished under different environmental conditions. Among them, liquid-phase exfoliation (LPE)^{2,3,5,11–15} is an attractive strategy, being extremely versatile and applicable to a variety of environments and on different substrates. While bottom-up methods, in particular CVD, can yield large size, LPE gives limited sheet sizes^{11,16–18}. Nevertheless, LPE has several advantages. It is a viable low-cost process, which can be easily upscaled to mass-produced dispersions processable by well-established techniques such as spin-coating, drop-casting, screen-printing and ink-jet printing¹⁷. Increasing research efforts are being devoted to the production of graphene via LPE to improve the material's physicochemical and electrical properties.

Small organic molecules, such as surfactants or dispersion-stabilizing agents, can promote the exfoliation of graphite into graphene in organic solvents^{5,11}, in particular when such molecules have higher adsorption energies on the basal plane of graphene than those involved in solvent–graphene interaction¹¹. We recently found that long alkanes are particularly suitable for enhancing the yield of exfoliation^{19,20}.

Photochromic molecules, in particular azobenzene-based molecules, covalently linked to reduced graphene oxide²¹, physisorbed directly on graphene^{22,23} or through pyrene anchoring groups²⁴ on the graphene surface, or even when graphene is adsorbed on an azobenzene self-assembled monolayer²⁵, can be used to reversibly modulate the graphene's electronic properties. Moreover, it was shown that covalent functionalization of gold surface²⁶ or carbon nanotubes²⁷ with azobenzene molecules can be used as a route for fabrication of light-driven electronic switches. Nonetheless, the use of additional responsive functions provided by a suitably designed molecule to assist the LPE of graphite into functional inks is still unexplored. This approach could lead to the production of functional hybrid materials and nanocomposites in a one-pot process.

Here we combine photochromic systems and LPE graphene exploiting the properties of these materials. We focus on a commercial alkoxy-substituted azobenzene, i.e., 4-(decyloxy)azobenzene. The presence of a long alkoxy side chain is expected to enhance the molecular interaction with graphene²⁸, and promote the exfoliation of graphite towards graphene. Here we demonstrate that the use of 4-(decyloxy)azobenzene has two major advantages: first, the amount of graphene dispersed in *N*-methyl-2-pyrrolidone (NMP) can be enhanced by exploiting the photoisomerization of 4-(decyloxy)azobenzene molecules during exfoliation. Second, the isomerization of 4-(decyloxy)azobenzene from *trans* to *cis* and vice versa, when physisorbed between adjacent graphene layers leads to

a reversible modulation of the inter-flake distance on the sub-Ångström scale. This is reflected in a light response of the electrical properties of the hybrid material.

Results

Liquid-phase exfoliation. To test the ability of alkoxy-substituted azobenzenes to increase Y_W (%), which is the yield of graphene exfoliation, defined as the ratio between the weight of dispersed graphitic material and that of the starting graphite flakes, as well as to exploit the photochromic nature of such molecules when interacting with graphene, vials containing NMP, graphite powder and azobenzene are exposed to tip sonication for 3 h (see Methods and Supplementary Note 1 for details). This experiment is carried out either in dark or under ultraviolet irradiation, using a portable ultraviolet lamp, at two temperatures: 20 and 40 °C (see experimental set-up in Supplementary Fig. 1). Subsequently, the dispersions are allowed to settle for 15 min, then decanted and centrifuged for 1 h at 10,000 r.p.m. Control samples are also prepared, consisting of dispersions prepared in the absence of 4-(decyloxy)azobenzene both in dark and irradiated at 365 nm at either 20 or 40 °C. To quantify the concentration of graphene after centrifugation, a mixture of graphene dispersion and 2-propanol (IPA) is first heated to 50 °C for 30 min and then passed through polytetrafluoroethylene membrane filters. The remaining solvent and weakly interacting 4-(decyloxy) azobenzene molecules are washed out several times with diethyl ether and IPA. Measurements of the filtered mass are performed on a microbalance to infer the concentration of graphitic material in dispersion, needed to quantify Y_W (%) (see Fig. 1b). The presence of adsorbed molecules may affect the mass measurements and Y_W (%). Thus, the heating step is necessary to completely desorb the 4-(decyloxy)azobenzene molecules, as proven with X-ray photoelectron spectroscopy (Supplementary Fig. 2 and Supplementary Note 2). By analysing 20 independent experiments, we find that when the exfoliation is performed in the absence of 4-(decyloxy)azobenzene (control experiments), comparable Y_W are observed when dispersions are kept at 20 °C (0.64%) or heated at 40 °C (0.62%). The irradiation at 365 nm does not affect Y_W , neither at 20 nor at 40 °C (0.63% in both cases).

LPE in the presence of alkoxy-substituted azobenzene acting as dispersion-stabilizing agent can undergo different mechanisms depending on the isomeric form of the photochromic molecule (Fig. 1c). In our case, the presence of 4-(decyloxy)azobenzene has no major influence on Y_W of dispersions prepared in dark (0.71% and 0.72% at 20 and 40 °C, respectively). As previously reported¹¹, the use of small organic molecules, in particular those based on aromatic cores¹¹ and alkyl functionalization^{19,20}, can promote graphene exfoliation because of their high affinity for the basal plane of graphene hindering interflake stacking. The relation between interaction energy and exfoliation yield is not straightforward. In some cases, molecules with lower adsorption energy on graphene give higher exfoliation yield, as demonstrated for graphite exfoliation²⁹, as well as for exfoliation of a wide range of other layered materials³⁰. This is because a critical step of the process is the adsorption of the molecule on the graphene surface and the displacement of the adsorbed solvent layer, overcoming an activation energy barrier that depends significantly on molecular structure and conformation. Therefore, even a minor increase of Y_W (0.06–0.09%) on addition of a small amount of 4-(decyloxy)azobenzene (5 wt%) highlights the importance of these molecules during LPE.

In contrast to the experiments performed in dark, irradiation with ultraviolet light at 365 nm increases the concentration of exfoliated material. At 20 °C we obtain $\sim 81 \pm 5 \mu\text{g ml}^{-1}$,

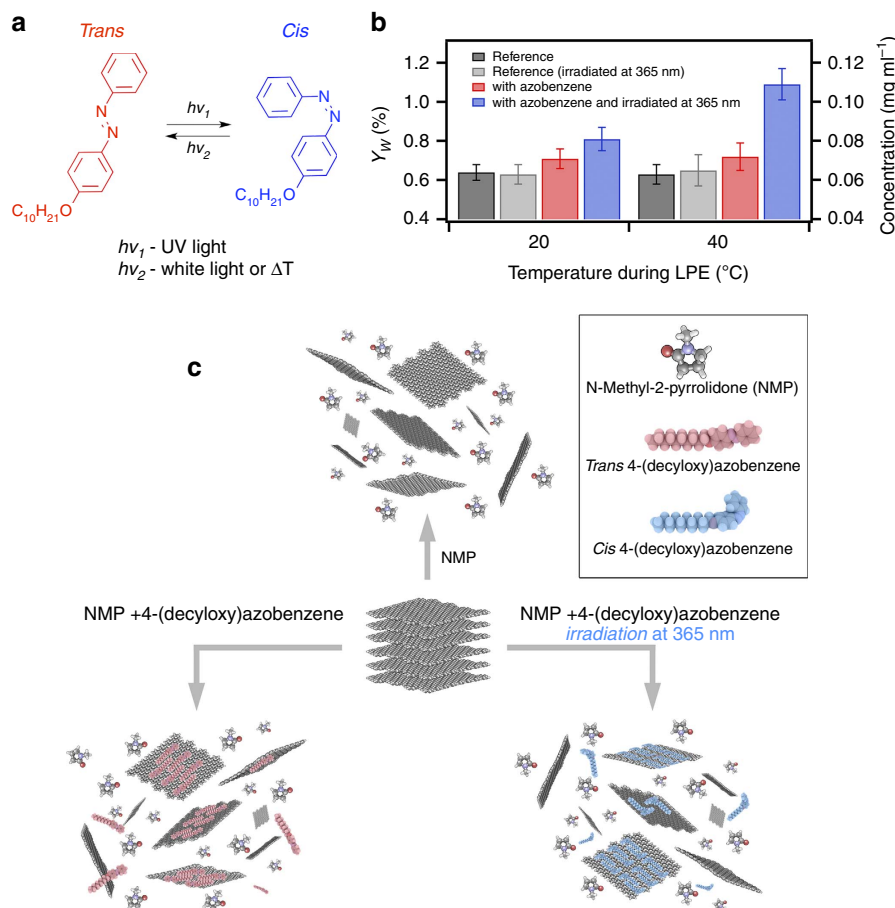


Figure 1 | Light-assisted graphene's LPE process in the presence of 4-(decyloxy)azobenzene and yield of exfoliation. (a) Chemical structure of 4-(decyloxy)azobenzene and reversible *trans-cis* photoisomerization under UV and visible light. (b) Y_W and concentration after filtration. The error bars reflect a statistical analysis on 20 independent experiments. (c) Schematic representation of the LPE process under different experimental conditions: in NMP (reference experiment); and in NMP with azobenzene in dark and under UV irradiation.

corresponding to $\sim 30\%$ increase in Y_W , when compared with reference samples ($63 \mu\text{g ml}^{-1}$). Yet, the largest increase in concentration is obtained by irradiating the dispersions heated at 40°C , reaching $110 \pm 8 \mu\text{g ml}^{-1}$, which corresponds to a 75% increase in Y_W . These results demonstrate that the addition of 4-(decyloxy)azobenzene during LPE leads to a significant increase in Y_W only in samples containing 4-(decyloxy)azobenzene irradiated at 365 nm. Molecules rapidly switching conformation, such as azobenzenes on ultraviolet (UV) illumination, heating and sonication, can overcome the activation barriers to adsorption, acting as 'nano-spinners' that disrupt the adsorbed solvent layer more effectively than molecules having a static conformation. Therefore, the increase in concentration can be attributed to the motion resulting by the *trans-to-cis* photoisomerization. The Y_W temperature dependence may be due to differences in molecule-graphene interactions at 20 and 40°C , as well as different kinetics of the *trans-to-cis* photoisomerization.

Trans-to-cis photoisomerization and cis-to-trans relaxation.

The transition from the thermodynamically stable *trans* to the metastable *cis* form can be induced by irradiation with UV light, and takes place on the picosecond timescale^{31,32}, whereas the *cis-to-trans* isomerization is typically triggered by irradiation with visible light or heat³³. The latter can also be activated by the use of ultrasound-induced mechanical force³³. Ref. 34 claimed

that mechanoisomerization of azobenzene typically results in the cleavage of the N = N azo bond. However, more recent theoretical calculations³⁵ and experiments³⁶ have challenged this view.

To gain a quantitative understanding of the photoisomerization of 4-(decyloxy)azobenzene, we perform a kinetic analysis of both *trans-to-cis* and *cis-to-trans* isomerization. The UV-visible spectrum of 4-(decyloxy)azobenzene dissolved in NMP (Fig. 2a, black line) shows an absorption maximum at 353 nm, arising from the $\pi-\pi^*$ transition³³, and a peak at 442 nm, due to $n-\pi^*$ transitions³³. The UV-visible spectrum of the above solution when irradiated at 365 nm shows a reduction of the $\pi-\pi^*$ transition band at 353 nm, and an increase in absorbance of the 442 nm ($n-\pi^*$ transition) peak, which is a characteristic feature of the *trans-to-cis* photoisomerization (Fig. 2a, red line; and Supplementary Fig. 3). The photostationary state can be reversibly converted back to the *trans* isomer on irradiation at 450 nm (see Methods for details). The yield of the conversion back to the thermodynamically stable *trans*-4-(decyloxy)azobenzene is higher than 95% (Fig. 2a, black dashed line).

To probe the *cis-to-trans* isomerization of the azobenzene molecules under experimental conditions corresponding to those used during the LPE process, i.e., at 20 and 40°C , in the presence of ultrasound-induced mechanical forces, a stock solution of 4-(decyloxy)azobenzene in NMP (16.2 mM) is prepared, and then exposed to 365 nm light and sonicated for 3 h (see Supplementary Note 1 for details). Every 30 min

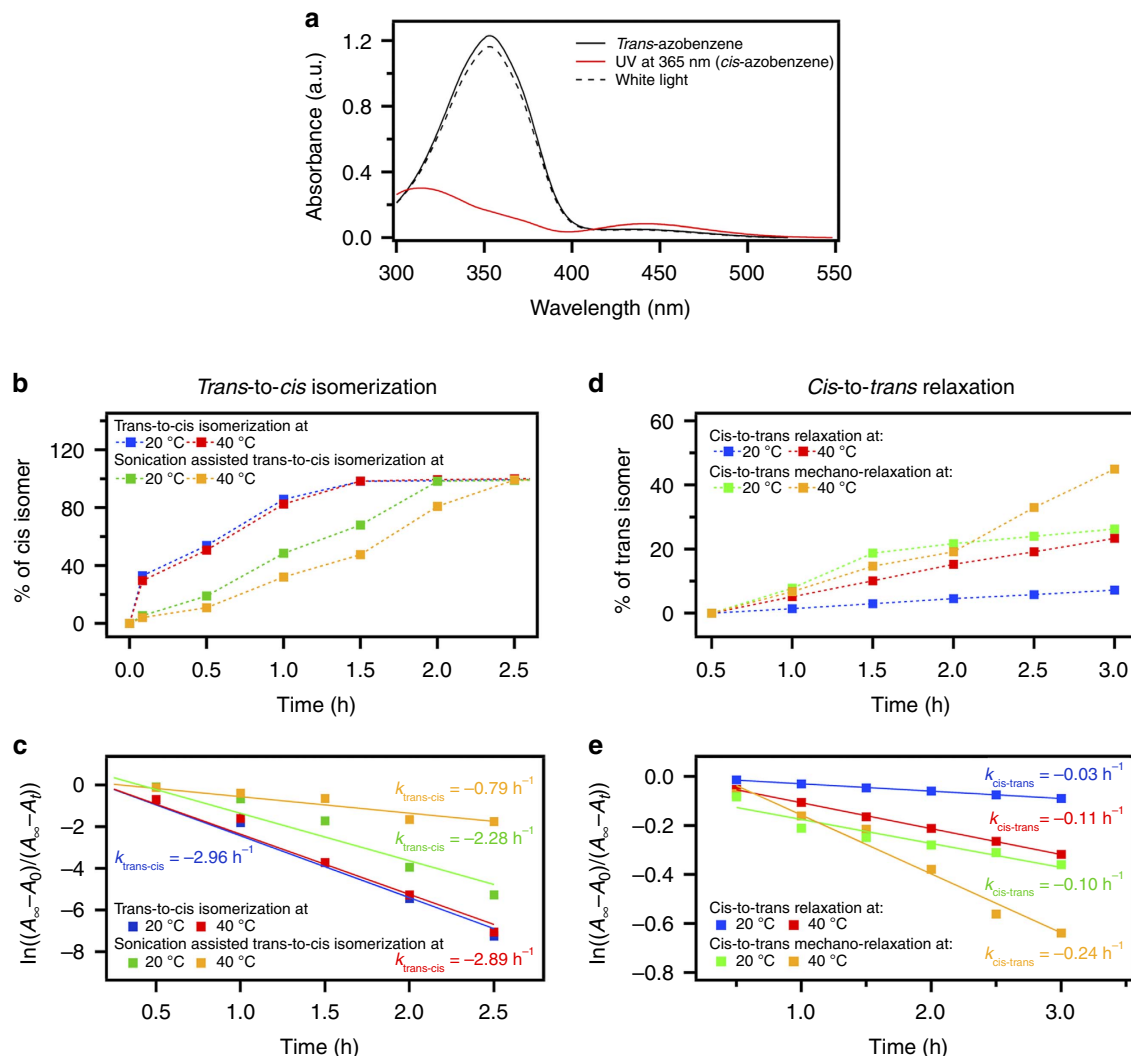


Figure 2 | Spectroscopic characterization of *trans*-to-*cis* isomerization and *cis*-to-*trans* relaxation. (a) UV-visible spectra of 4-(decyloxy)azobenzene in NMP (1.62 mM) showing the disappearance of the 353-nm band and an increase of the 442-nm band for 365-nm irradiation. The solid black line corresponds to the parent *trans*-4-(decyloxy)azobenzene spectrum, the red line represents a typical spectrum of a solution irradiated with UV light (*cis*-4-(decyloxy)azobenzene), whereas the black dashed line corresponds to a *cis*-4-(decyloxy)azobenzene solution irradiated with visible light (thus re-transformed into *trans*-4-(decyloxy)azobenzene). (b) Conversion percentage from *trans* to *cis* as a function of UV irradiation time at 20 and 40 °C. (c) First-order kinetic plots and rate constants ($k_{\text{trans-cis}}$) for *trans*-to-*cis* isomerization at 20 and 40 °C. (d) Conversion percentage from *cis* to *trans* as a function of time at 20 and 40 °C. (e) First-order kinetic plots and rate constants ($k_{\text{cis-trans}}$) for the *cis*-to-*trans* relaxation at 20 and 40 °C. (b-e) Reference samples prepared without sonication: blue (20 °C) and red (40 °C); sonicated samples: green (20 °C) and orange (40 °C).

(except for a first measurement performed after 5 min) 0.2 ml of UV-irradiated solution is transferred (in the dark) into a quartz cuvette, diluted 10 times with NMP. The optical absorption spectrum is then recorded (shown in Supplementary Fig. 4). Finally, to ensure the stability of the azo bond during sonication, a solution sonicated for 3 h is exposed to white light and an absorption spectrum is recorded. A similar procedure is applied for blank experiments, i.e., in the absence of ultrasound-induced mechanical forces.

Analysis of the absorption and proton nuclear magnetic resonance spectra (Supplementary Fig. 5) acquired for different experimental conditions allows us to quantify the percentage of conversion from *trans*- to *cis*-4-(decyloxy)azobenzene, as well as the rate constants for *trans*-to-*cis* isomerization. Both nuclear magnetic resonance and high-performance liquid chromatography data (Supplementary Figs 5 and 6, and Supplementary Note 3) show that the decyloxy chains are not

being chopped from the azobenzene core. The slow kinetics of the *trans*-to-*cis* isomerization can be explained by the fact that both spectroscopic experiments and LPE process are carried out under unusual isomerization conditions, including a low UV light power density (0.34 mW cm^{-2}). A different time (30 min) is needed for reaching a photostationary state, in the reference and sonicated samples, as displayed in Fig. 2b. Previous studies^{36,37} on the *trans*-to-*cis* isomerization of azobenzene in the presence of UV light showed that the reaction follows first-order kinetics and the rate constant k can be written as follows:

$$\ln \left(\frac{A_{\infty} - A_t}{A_{\infty} - A_0} \right) = -kt \quad (1)$$

where A_0 , A_t and A_{∞} are the absorbances before irradiation, at irradiation time t and after irradiation for a prolonged time (ca. 6 h). Applying equation (1), we find that the isomerization constant $k_{\text{trans-cis}}$ at 20 °C for the 4-(decyloxy)azobenzene linked

to graphene is similar to $k_{trans-cis}$ at 40 °C: 2.96 and 2.89 h⁻¹, respectively. Significantly different $k_{trans-cis}$ kinetics are observed for the samples exposed to ultrasound-induced mechanical forces, i.e., 2.28 and 0.79 h⁻¹ for dispersions prepared at 20 and 40 °C, respectively. To ensure the stability of the azo bond during sonication, the two samples are exposed to white light, and the absorption spectra recorded. The absorption at 365 nm is consistent with the *trans*-4-(decyloxy)azobenzene spectra in both cases (Supplementary Figs 3 and 4), indicating that the molecules, in particular the azo bond, are stable during sonication at various temperatures.

Since the *trans*-to-*cis* isomerization and the LPE processes are performed under UV light, the possible *cis*-to-*trans* back-conversion can be considered promoted by thermal or mechano-thermal relaxation, for experiments performed in the absence or presence of ultrasound-induced forces, respectively.

To probe both thermal and mechano-thermal isomerization, four solutions (16.2 mM) are prepared in NMP and the UV-visible spectra recorded. The solutions are then irradiated with UV light (365 nm) for 3 h to photoisomerize the 4-(decyloxy)azobenzene from its *trans* to *cis* configuration (Supplementary Fig. 3). The solutions are then kept for 3 h at 20 and/or 40 °C, in the presence and/or absence of ultrasound-induced mechanical forces. Every 30 min, 0.2 ml of solution is transferred (in dark) onto a quartz cuvette and diluted 10 times with NMP. Absorption spectra are then recorded. Owing to the lack of white light during the 3 h relaxation, 4-(decyloxy)azobenzene molecules do not convert fully from their *cis*- to *trans*-isomers. As shown in Fig. 2c, the percentage of *cis*-to-*trans* conversion in the blank samples (without sonication) at 20 and 40 °C is ~8.6% and 27.6%, respectively. In contrast, the ultrasound-induced conversion is much higher, i.e., 29.8% and 51.2% for samples kept at 20 and 40 °C, respectively. Similar to the *trans*-to-*cis* isomerization, the *cis*-to-*trans* relaxation of 4-(decyloxy)azobenzene follows first-order kinetics, and k can be obtained from equation (1). $k_{cis-trans}$ for 4-(decyloxy)azobenzene kept at 20 °C is lower than $k_{cis-trans}$ for 4-(decyloxy)azobenzene relaxed at 40 °C, i.e., 0.03 and 0.11 h⁻¹, respectively (Fig. 2d). Notably different $k_{cis-trans}$ are also observed for samples exposed to ultrasound-induced mechanical forces, i.e., 0.10 and 0.24 h⁻¹ for dispersions kept at 20 and 40 °C, respectively.

These results indicate that the *trans*-to-*cis* isomerization of 4-(decyloxy)azobenzene strongly depends on the experimental

conditions. In particular, it is hindered by ultrasound-induced mechanical forces, which most likely cause the occurrence of the competing *cis*-to-*trans* isomerization. Furthermore, comparison of $k_{trans-cis}$ and $k_{cis-trans}$ at 20 and 40 °C reveals that, at higher temperature, the process is more dynamic. As a result, the higher concentration of flakes (110 μg ml⁻¹) obtained at 40 °C can be attributed to the dynamic conformational *trans*-to-*cis* and *cis*-to-*trans* changes of 4-(decyloxy)azobenzene molecules triggered simultaneously by the competing effect activated by UV light, temperature and ultrasounds.

Analysis of dispersions. To fully characterize the exfoliated flakes, both qualitative and quantitative information are required. While quantitative insights can be assessed by providing the Y_W , a qualitative analysis must give more relevant details, such as the percentage of single-layer graphene (SLG) and multi-layer graphene (MLG) flakes, the lateral size of the flakes and the presence/absence of defects. The number of graphene layers (N) can be quantified using high resolution-transmission electron microscopy (HR-TEM)^{3,5} and Raman spectroscopy^{17,18}. Together with the information coming from electron diffraction patterns, in HR-TEM N can be directly counted by analysing the folded edges³⁸. We focus on the samples prepared by LPE at 40 °C in the presence of azobenzene, while irradiating with UV light (highest increase in Y_W), and compare them with those exfoliated in NMP at 40 °C under UV irradiation (in the absence of azobenzene). The statistical analyses of N and the lateral flake size are reported in Supplementary Fig. 7a,b, respectively (Supplementary Note 4). In terms of N , minor differences are observed between the reference sample and flakes exfoliated in the presence of azobenzene molecules, where the percentage of SLG amounts to 20% and 14%, respectively. The lateral size of the flakes is not affected by the presence of azobenzene molecules during LPE (Supplementary Fig. 7b). Representative HR-TEM micrographs are reported in Supplementary Figs 8, 9 and 10.

The Raman spectrum of graphite and MLG consists of two fundamentally different sets of peaks. Those, such as D, G and 2D, present also in SLG, due to in-plane vibrations³⁹⁻⁴¹, and others such as the shear (C) modes⁴² and the layer-breathing modes (LBM)^{40,43}, due to the relative motions of the planes themselves, are either perpendicular or parallel to their normal. The G peak corresponds to the high-frequency E_{2g} phonon at Γ .

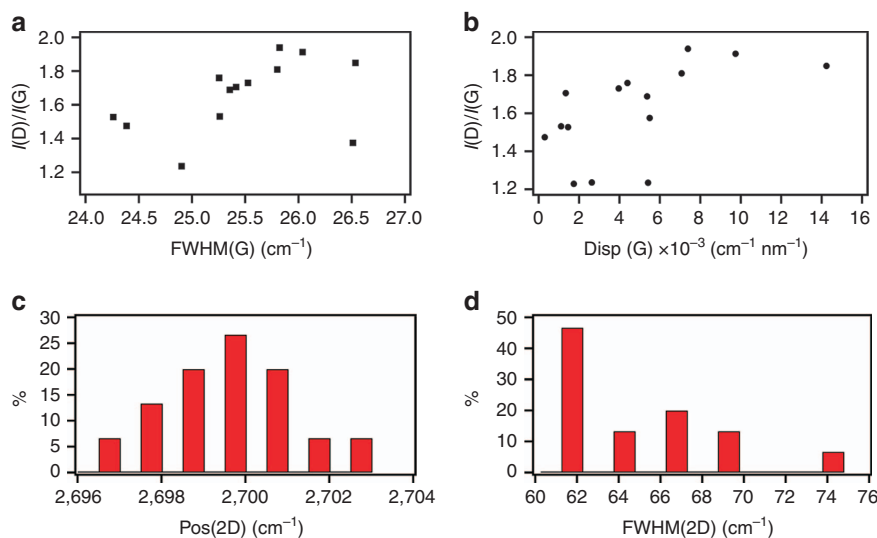


Figure 3 | Raman analysis of graphene/4-(decyloxy)azobenzene films. $I(D)/I(G)$ as a function of (a) $FWHM(G)$ and (b) $Disp(G)$. Distribution of (c) $Pos(2D)$ and (d) $FWHM(2D)$.

The D peak is due to the breathing modes of six-atom rings and requires a defect for its activation^{41,44,45}. It comes from transverse optical phonons around the Brillouin Zone edge **K** (refs 41,45), is active by double resonance⁴⁶ and is strongly dispersive with excitation energy due to a Kohn anomaly at **K** (ref. 47). Double resonance can also happen as intra-valley process, i.e., connecting two points belonging to the same cone around **K** or **K'**. This gives the so-called D' peak. The 2D peak is the D peak overtone while the 2D' peak is the D' overtone. Since 2D and 2D' originate from a process where momentum conservation is satisfied by two phonons with opposite wave vectors, no defects are required for their activation, and are thus always present³⁸. The 2D peak is composed of a single Lorentzian in SLG, whereas it splits into several components as *N* increases, reflecting the evolution of the electronic band structure³⁸.

In disordered carbons, the G peak position, Pos(G), increases as the excitation wavelength decreases from infrared to ultraviolet⁴⁴. Therefore, the dispersion of the G peak, Disp(G), i.e. the rate of change of Pos(G) with the laser excitation wavelength, increases with disorder⁴⁴. Similar to Disp(G), also the full width at half maximum of the G peak, FWHM(G), always increases with disorder⁴⁴. The analysis of the intensity ratio of the D and G peaks, $I(D)/I(G)$, combined with that of FWHM(G) and Disp(G) allows us to discriminate between disorder localized at the edges and disorder in the bulk of the samples. In the latter case, a higher $I(D)/I(G)$ would correspond to higher FWHM(G) and Disp(G).

Raman measurements are done on the same set of samples to characterize the quality of the graphitic material. Figure 3a,b show a small correlation between these parameters. This implies that the D peak is mostly due to edges, as well as the presence of some defects in the samples. FWHM(2D) (Fig. 3d) is larger with respect to that of graphene flakes produced by micromechanical cleavage, but still has a single Lorentzian line shape. This is consistent with the presence of MLGs composed of folded or juxtaposed SLGs, but still electronically decoupled¹⁷.

Figure 4a plots the Raman spectra of a graphene–azobenzene film after visible and UV light illumination, acquired at 514.5 nm with power <250 μW to avoid any Raman laser-induced isomerization of azobenzene. None of the graphene Raman

parameters show significant change on UV or visible light irradiation indicating negligible change in the defects and doping.

The *trans*-to-*cis* isomerization can also be monitored by Raman spectroscopy^{24,48}. Figure 4b plots the Raman spectrum of azobenzene after both visible and UV light illumination. The spectrum is composed of five main peaks, labelled C1–C5 (ref. 48). These can also be seen on the spectra of the graphene–azobenzene hybrids (Fig. 4c). The intensity ratio of peaks C3 and C4 can be used to monitor the isomerization of azobenzene as described in ref. 48. On illumination with visible light, the photochromic molecules fall into the *trans* configuration and $I(C3)/I(C4)$ approaches ~1. When the sample is illuminated with UV light, azobenzene molecules undergo *trans*-to-*cis* isomerization and $I(C3)/I(C4)$ decreases markedly. The effect is fully reversible and the *trans* form is recovered by a further visible light exposure as shown in Fig. 4d.

X-ray analysis. Powder X-ray diffraction is further used to characterize the structure of the graphene–azobenzene hybrid powder and to compare it with the control samples (Supplementary Note 5). Similarly to graphite, the powder prepared from LPE has a sharp peak at 26.7°, corresponding to an interlayer spacing of ~0.33 nm (Supplementary Fig. 11a). The X-ray diffraction patterns of powders prepared from graphene/*trans*-azobenzene and graphene/*cis*-azobenzene show new peaks at $2\theta = 12.3^\circ$ ($d_{\text{spacing}} \sim 0.72$ nm) and 9.9° ($d_{\text{spacing}} \sim 0.89$ nm), respectively (Supplementary Fig. 11b,c). This confirms that *trans* and/or *cis*-azobenzenes can sandwich between graphene layers, thus increasing the overall spacing.

Electrical characterization. To probe the electrical properties of the graphene–azobenzene hybrid and, in particular, to explore the potential light-responsive nature of the material, we drop-cast a ~100-nm-thick graphene–azobenzene film on a $n^+ + \text{Si}/\text{SiO}_2$ substrates exposing pre-patterned interdigitated gold electrodes (channel length = 10 μm; Fig. 6a,b).

Typical *I*-*V* curves exhibit a nonlinear resistive behaviour, as shown in Fig. 5c. The conductivity of the graphene–azobenzene hybrid is lower than that measured in control devices, i.e.,

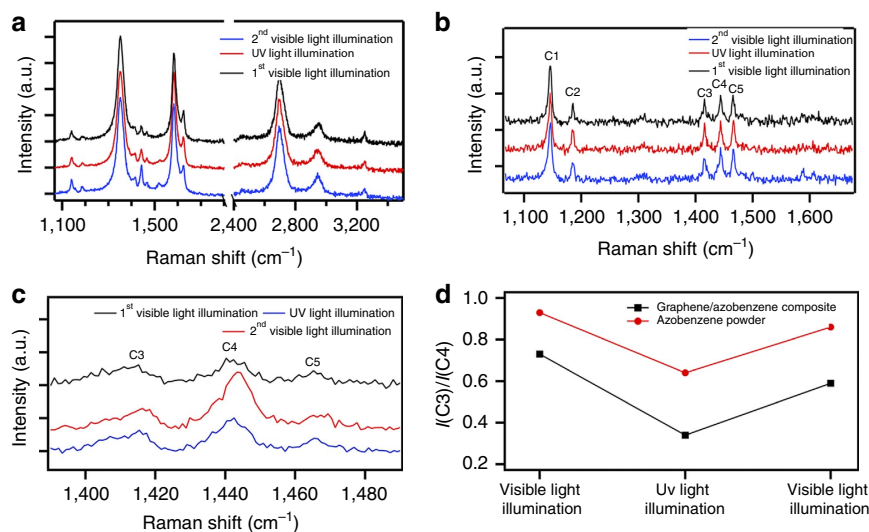


Figure 4 | Evolution of Raman spectra on illumination. (a) Comparison of the Raman spectrum of a graphene/4-(decyloxy) azobenzene hybrid film after 90-min illumination with visible light, UV light and visible light again to probe the effect of isomerization. (b) The same experiment on azobenzene powder. (c) 4-(decyloxy)azobenzene Raman peaks C3, C4 and C5 extracted from graphs in a showing the change of peaks ratio on illumination, which confirms the isomerization. (d) Dependence upon illumination of $I(C3)/I(C4)$ for both hybrid material and powders.

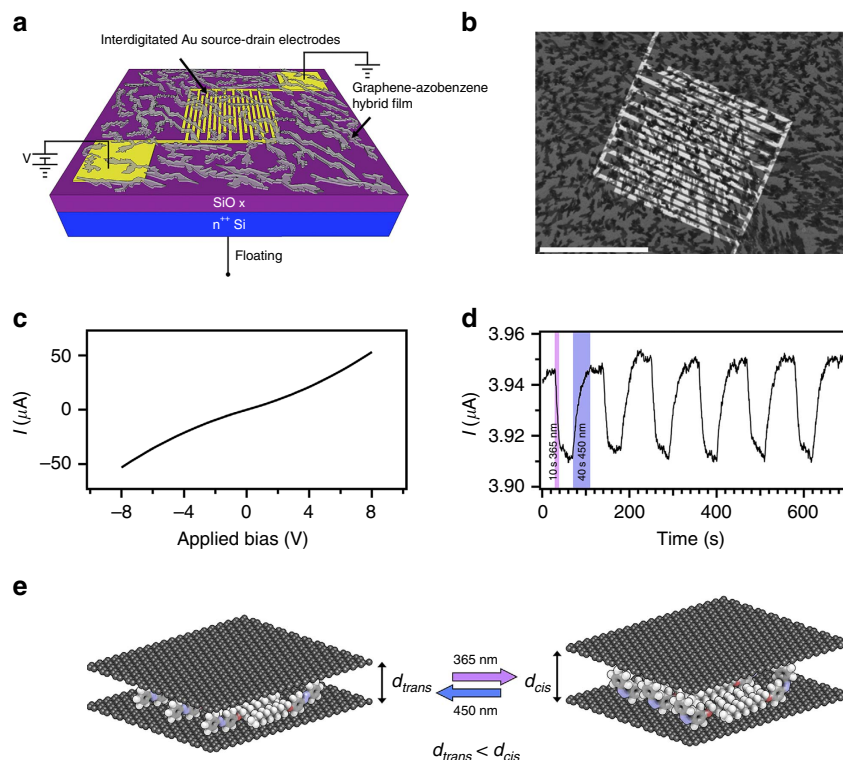


Figure 5 | Electrical characteristics of hybrid materials. (a) Scheme of the two-terminal device configuration, (b) scanning electron microscopy image of interdigitated Au electrodes covered with a hybrid film. Scale bar, 500 μm . (c) I - V characteristics, (d) optical modulation of current response for a static bias and dynamic alternative UV and visible light irradiation cycles. (e) Schematic of graphene-azobenzene hybrid undergoing UV and visible irradiation cycles.

comprising as active layer graphene exfoliated in NMP in the absence of azobenzene (Supplementary Fig. 12). Figure 6d shows the current modulation in a two-terminal device with graphene-azobenzene on cycles of UV and visible light irradiation, for 1 V applied between the two electrodes. One cycle consists of 10-s UV light (365 nm), 1-min rest in dark followed by 40-s visible light (450 nm) irradiation. Under UV exposure (magenta background) a current decrease is detected, which reversibly increases to about the initial value under visible light irradiation (violet background) over various cycles. No fatigue is observed during six cycles of photoisomerization. Conversely, the control devices show no response to light (Supplementary Fig. 12). Noteworthy, in some cases the increase of current in the hybrid films can be the result of π -electron interactions between the molecules and graphene⁴⁹; however, such phenomenon, known as increased photoconductivity, is irreversible and can only be modulated by varying the ratio between graphene and *ad hoc* molecules.

In the azobenzene-graphene film (Supplementary Figs 13 and 14), the molecules are physisorbed on top and in between the graphene sheets. Under UV irradiation, the azobenzene molecules undergo a conformational change from the less-bulky *trans* isomer to the bulkier *cis* isomer. Such a process is therefore accompanied by an increase in the few-layer graphene (FLG) inter-sheet distance, thereby hindering the charge transport via hopping between the sheets, resulting in lower conductivity of the hybrid film. The conductivity of the hybrid material can be fully restored by irradiating with visible light, causing the *cis*-to-*trans* photoisomerization.

To gain greater insight into the conduction mechanism and the effect of isomerization, we then perform Kelvin probe measurements (Supplementary Note 6). We find that the work function is reversibly photo-modulated over various cycles (Supplementary Fig. 15), providing further evidence for the isomerization of the

azobenzene molecules. This difference in work function has a direct effect on charge injection from the electrodes to the graphene/azobenzene conductive material, which is less favourable in the presence of the *cis* isomer. Light modulation can be applied multiple times to the systems, with no evidence of decrease in performance. We assign this to graphene's shielding of the azobenzene molecules from the outer environment. An ideal case consists of stacks of alternating graphene and azobenzenes, the latter having a thickness, which can be photo-modulated (Fig. 5e). In reality, the flakes (with average lateral sizes of 200 nm) form aggregates possessing a poor degree of order. Within these aggregates the azobenzenes are intercalated in between adjacent layers of graphene. The control samples show no change in work function on UV and visible light cycling (Supplementary Fig. 15).

Molecular modelling simulations. To gain a better understanding of the interactions of the azobenzene molecules with graphene, we perform molecular dynamics simulations (see Supplementary Note 7 for details). All calculations are done using the Groningen Machine for Chemical Simulations (GROMACS)⁵⁰ package and a modified version of the all-atom Optimized Potentials for Liquid Simulations (OPLSAA) force field developed for azobenzenes^{51,52}. To assess the relative adsorption affinity of the *trans* versus *cis* conformations, we first compute the interaction energy for a single azobenzene molecule by running a 1-ns simulation in vacuum. The graphene layer is taken as an infinite rigid body in these calculations. The computed interaction energies of -130.1 ± 7.5 and $-115.7 \pm 8.0 \text{ kJ mol}^{-1}$ for *trans*- and *cis*-azobenzene, respectively, are consistent with the expected stronger adsorption of *trans*-azobenzene, resulting from its planar geometry and the concomitant maximized π - π interactions between the phenyl

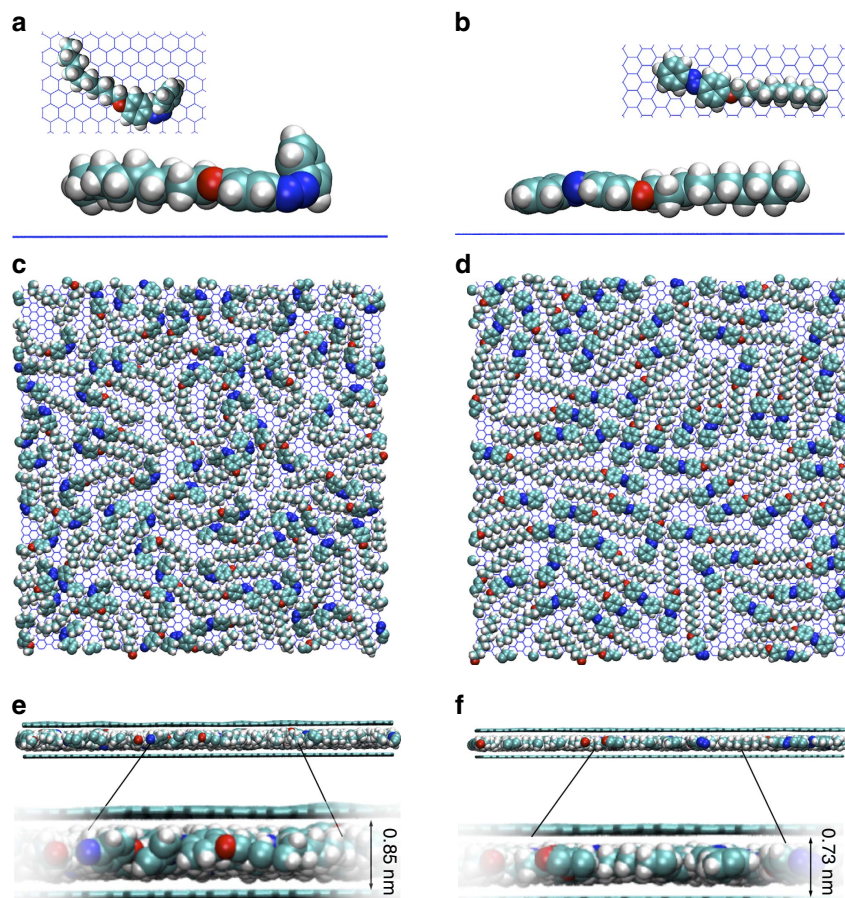


Figure 6 | Molecular modelling of graphene interaction with *cis* and *trans* azobenzene. Side and top views of a single (a) *cis*- and (b) *trans*-azobenzene molecule adsorbed on SLG. Top view of the (c) *cis* and (d) *trans*-monolayer, and side view of the molecular system consisting of the (e) *cis* and (f) *trans*-monolayer sandwiched between two SLGs, with the indication of the SLGs separation.

groups and graphene. The average adsorption distance for the *trans* molecule is ~ 0.07 nm shorter than *cis* (0.34 versus 0.41 nm). Figure 6a,b plots top and side views of the adsorbed *cis* and *trans* molecules from the last snapshots along the molecular dynamics trajectories.

It should be noted that the conformation giving the higher exfoliation yield is the *cis* one, with lower interaction energy with graphene (14.4 kJ mol^{-1} difference). This counterintuitive finding highlights the importance of kinetic factors on exfoliation yield rather than thermodynamic factors, in good agreement with previous results obtained with rigid molecules^{29,30}. The 70% increase in exfoliation yield could be due to the rapid, dynamic change of conformation between *cis* and *trans* that the molecules undergo during the exfoliation, which is more rapid at high temperature and under sonication (Fig. 2).

We then study the supramolecular organization of *trans*- and *cis*-azobenzenes on SLG in vacuum. In the absence of experimental structural data, we consider highly regular self-assembled monolayers (Supplementary Fig. 16) and test their stability by performing simulations of the assemblies at room temperature. The regular assemblies are unstable at 300 K and disassemble after few tens of picoseconds, suggesting that the azobenzene molecules form disordered layers at the SLG surface. To investigate the formation and structure of such disordered layers, we use the following protocol. Azobenzene molecules are introduced one by one in the simulation box at a distance of 1.8 nm above the plane of the infinite SLG with a random orientation. The initial atomic velocities are assigned so that the resulting vectors point towards the SLG, thereby prompting

physical adsorption on the surface. Room-temperature molecular dynamics simulations of a few hundreds of picoseconds are then performed to explore the configurational space after each molecular deposition, and the last saved configuration is used as input for the landing of the subsequent molecule. The scheme is iterated multiple times until the desired surface coverage is reached. A 5-ns simulation is then performed on the final structure to equilibrate the monolayer at room temperature. A more detailed description of the methodology is provided in Supplementary Note 8. Full coverage of the graphene periodic layer of 115.8 nm^2 is reached when 64 (72) molecules of *trans* (*cis*)-azobenzene are adsorbed, which translates into a surface contact area on graphene of $\sim 1.8 \text{ nm}^2$ for the *trans* and $\sim 1.6 \text{ nm}^2$ for the *cis* conformation. Figure 6c,d plots a top view of the azobenzene monolayers obtained for the two conformers in the case of full coverage. Supplementary Figs 17 and 18 show the formation of those monolayers as a function of the number of molecules adsorbed on SLG.

To validate the hypothesis that the insertion of a *trans*-/*cis*-monolayer sandwiched between two SLGs can result in different interlayer spacing according to the ideal model, a second SLG is placed on top of the azobenzene monolayers prepared using the deposition protocol described above. The 1-ns simulations are then done at room temperature. The results show that *cis*-azobenzenes maintain the SLG at a distance ~ 0.85 nm, while the layer separation decreases to ~ 0.73 nm for *trans* (Fig. 6e,f), in excellent agreement with the X-ray data. This supports the view that photoisomerization of the molecules from *trans* to *cis* can favour the exfoliation process. To investigate

the effect of this switchable separation on charge transport, we perform quantum chemical calculations (at the intermediate neglect of differential overlap level⁵³) on two square-shaped nanographenes ($\sim 20 \text{ nm}^2$) interacting either through-space or in the presence of the sandwiched (*trans* or *cis*) azobenzenes (Supplementary Fig. 19). In the first case (no sandwiched layer), the electronic couplings mediating positive and negative charge carrier tunnelling from one nanographene to the other, as obtained from the diabaticization scheme reported in ref. 54, decrease by a factor ~ 100 when the interlayer distance is increased from 0.73 (corresponding to the azobenzenes in *trans* conformation) to 0.85 nm (*cis* conformation). In both cases, these interactions are very small due to the fast fall-off decay of the nanographene wavefunction overlap. Interestingly, the corresponding couplings calculated in the presence of the sandwiched azobenzenes are several orders of magnitude larger and show a less pronounced change (by a factor ~ 10) on photoisomerization, suggesting that the loss in electrical transmission associated with the larger inter-graphene distances is at least partly compensated by conformational-dependent superexchange effects involving the molecular orbitals of the azobenzenes. Our experimental current modulation on photoisomerization of azobenzenes (Fig. 5d) is much smaller than the calculated one (factor ~ 100). This can be understood considering that the simulations are run for two SLG intercalated by a tightly packed, physisorbed, self-assembled layer of azobenzene, whereas the experiments are done for hybrid films with a distribution of layer thicknesses (Supplementary Fig. 7a) separated by a small quantity of azobenzene (below 5% of the area of graphene).

As aforementioned the ideal model does not fully describe our real system that consists of poorly ordered aggregates comprising flakes intercalated with azobenzenes, and charges hopping between adjacent graphenes. The distance between the adjacent graphene sheets can be varied on photoisomerization of the azobenzenes.

Discussion

We demonstrated that alkoxy-substituted photochromic molecules can act as photo-addressable surfactant and as dispersion-stabilizing agents to enhance the yield of exfoliation in an upscalable molecule-assisted LPE-based method. The simultaneous use of UV light, promoting the *trans*-to-*cis* isomerization, as well as thermal annealing at 40 °C and mechanical forces generated by sonication, both favouring *cis*-to-*trans* isomerization, promotes the exfoliation in liquid media. The most effective exfoliation is obtained with azobenzene molecules irradiated with UV light in NMP at 40 °C, with a concentration of exfoliated graphene of $110 \mu\text{g ml}^{-1}$. This corresponds to an $\sim 80\%$ increase in exfoliation yield when compared with pure NMP ($63 \mu\text{g ml}^{-1}$). By depositing the hybrid film onto Au pre-patterned SiO_2 substrates, light-responsive thin hybrid films, formed in a one-step co-deposition process, can be realized, whose conductivity can be reversibly modulated by the *trans*-*cis* photoisomerization of the azobenzenes. By combining this approach with cost-effective techniques, such as ink-jet printing, more complex responsive device designs and architectures may be realized. This paves the way to future applications such as optically controllable memory switch elements for light-assisted programming and photosensors.

Methods

Materials. Graphite synthetic flakes (Product No. 332461), 4-(decyloxy) azobenzene (Product No. S931950) and NMP (Product No. 270458) are sourced from Sigma-Aldrich.

Liquid-phase exfoliation. Graphene dispersions are prepared by adding graphite powder (100 mg) to NMP (10 ml), and tip-sonication (Labsonic M, Platinum tip, diameter 2 mm, sound rating density 300 W cm^{-2}) for 3 h either in dark or under UV light irradiation, using a portable laboratory ultraviolet lamp (8 W, 365 nm, 0.34 mW cm^{-2} , Herolab GmbH), in glass vials (Pyrex), in the presence of azobenzene molecules (5.5 mg). The dispersions are then allowed to settle for 15 min, then decanted and centrifuged (Eppendorf, centrifuge 5804) for 1 hour at 10,000 r.p.m. From the centrifuged dispersions 70 vol% are pipetted off the top for characterization and film deposition. To quantify the concentration of flakes after centrifugation, the dispersions are passed through polytetrafluoroethylene membrane filters (pore size 100 nm). Measurements of the filtered mass are performed with a microbalance (Sartorius MSA2.75).

Device fabrication. n^{++} Si substrates with a thermally grown SiO_2 layer (230 nm) and pre-patterned interdigitated gold source and drain electrodes (IPMS Fraunhofer) with different channel length ($L = 2.5, 5, 10$ and $20 \mu\text{m}$) and constant channel width ($W = 10 \text{ mm}$) are used. The substrates are cleaned before device fabrication in an ultrasonic bath (FB 15047, Fisher Scientific) of acetone and isopropanol, 15 min in each solvent, and treated 5 min (+ 30 min incubation) with an UV surface decontamination system (PSD-UV, Novascan) to improve wetting of the solvent. The dispersions (50 μl) are drop-cast on clean substrates and dried for 48 h in vacuum at 30 °C.

Characterization. The electrical characterization is carried out in inert atmosphere (glovebox) with an electrometer (Keithley 2636A) interfaced with LabTracer software. For the light-induced switch, a Polychrome V monochromator (Till Photonics) is used as ultraviolet light (350 nm , 5.64 mW cm^{-2}) and visible light source (450 nm , 4.83 mW cm^{-2}). For the Raman experiments, graphene dispersions are drop-cast onto pre-cleaned n^{++} Si substrates with a thermally grown SiO_2 layer (300 nm) and dried for 48 h. Raman spectra are collected with a Renishaw InVia spectrometer at 457, 514.5 and 633 nm. The excitation power is kept below 1 mW to avoid the effects of local heating. The scattered light is collected with a $\times 100$ objective. HR-TEM is done in a FEI Tecnai F20 equipped with a Schottky emitter and operated at 120 keV primary beam energy. Scanning electron microscopy images are recorded with a Quanta FEG 250 from FEI.

The thickness of the hybrid films is determined with an Alpha-Step IQ Surface Profiler from KLA Tencor. X-ray photoelectron spectroscopy analyses are carried out on a Thermo Scientific K-Alpha X-ray photoelectron spectrometer, with a basic chamber pressure $\sim 10^{-8}$ mbar and an Al anode as the X-ray source (X-ray radiation of 1,486 eV). Spot sizes of 400 μm , pass energies of 200 eV for survey scans and 50 eV for high-resolution scans are used. A volume of 150 μl of the dispersions are spin-coated on Au substrate for 1 min at 1,000 r.p.m. and substrates are annealed for 1 day at 100 °C in a oven under vacuum. Samples for X-ray diffraction are prepared by precipitating graphene and/or graphene/azobenzene by adding water:ethanol (1:1, vol:vol) into NMP. The collected precipitate is dried under vacuum for 24 h. The powder X-ray diffraction patterns are obtained using a Bruker AXS D2 Phaser (LYNXEYE detector) with Ni-filtrated Cu-K α radiation ($\lambda = 1.5406 \text{ \AA}$) with a 1-mm air-scattering slit and 0.1-mm equatorial slit. Samples are deposited on the surface of a single crystal Si wafer (cut of (911)). X-ray diffraction patterns are collected with 0.016° steps and 10 s per step increments from 8° to 80°.

References

- Geim, A. K. & Novoselov, K. S. The rise of graphene. *Nat. Mater.* **6**, 183–191 (2007).
- Ferrari, A. C. *et al.* Science and technology roadmap for graphene, related two-dimensional crystals, and hybrid systems. *Nanoscale* **7**, 4598–4810 (2015).
- Bonaccorso, F. *et al.* Production and processing of graphene and 2d crystals. *Mater. Today* **15**, 564–589 (2012).
- Narita, A. *et al.* Synthesis of structurally well-defined and liquid-phase-processable graphene nanoribbons. *Nat. Chem.* **6**, 126–132 (2014).
- Hernandez, Y. *et al.* High-yield production of graphene by liquid-phase exfoliation of graphite. *Nat. Nanotechnol.* **3**, 563–568 (2008).
- Chen, L., Hernandez, Y., Feng, X. L. & Müllen, K. From nanographene and graphene nanoribbons to graphene sheets: chemical synthesis. *Angew. Chem. Int. Ed.* **51**, 7640–7654 (2012).
- Palma, C.-A. & Samori, P. Blueprinting macromolecular electronics. *Nat. Chem.* **3**, 431–436 (2011).
- Kim, K. S. *et al.* Large-scale pattern growth of graphene films for stretchable transparent electrodes. *Nature* **457**, 706–710 (2009).
- Li, X. S. *et al.* Large-area synthesis of high-quality and uniform graphene films on copper foils. *Science* **324**, 1312–1314 (2009).
- Berger, C. *et al.* Electronic confinement and coherence in patterned epitaxial graphene. *Science* **312**, 1191–1196 (2006).
- Ciesielski, A. & Samori, P. Graphene via sonication assisted liquid-phase exfoliation. *Chem. Soc. Rev.* **43**, 381–398 (2014).

12. Parvez, K. *et al.* Electrochemically exfoliated graphene as solution-processable, highly conductive electrodes for organic electronics. *ACS Nano* **7**, 3598–3606 (2013).
13. Parvez, K. *et al.* Exfoliation of graphite into graphene in aqueous solutions of inorganic salts. *J. Am. Chem. Soc.* **136**, 6083–6091 (2014).
14. León, V. *et al.* Few-layer graphenes from ball-milling of graphite with melamine. *Chem. Commun.* **47**, 10936–10938 (2011).
15. Sampath, S. *et al.* Direct exfoliation of graphite to graphene in aqueous media with diazaperopyrenium dications. *Adv. Mater.* **25**, 2740–2745 (2013).
16. Coleman, J. N. Liquid exfoliation of defect-free graphene. *Acc. Chem. Res.* **46**, 14–22 (2013).
17. Torrisi, F. *et al.* Inkjet-printed graphene electronics. *ACS Nano* **6**, 2992–3006 (2012).
18. Marago, O. M. *et al.* Brownian motion of graphene. *ACS Nano* **4**, 7515–7523 (2010).
19. Ciesielski, A. *et al.* Liquid-phase exfoliation of graphene using intercalating compounds: a supramolecular approach. *Angew. Chem. Int. Ed.* **53**, 10355–10361 (2014).
20. Haar, S. *et al.* A supramolecular strategy to leverage the liquid-phase exfoliation of graphene in the presence of surfactants: unraveling the role of the length of fatty acids. *Small* **11**, 1691–1702 (2014).
21. Luo, W. *et al.* A high energy density azobenzene/graphene hybrid: a nano-templated platform for solar thermal storage. *J. Mater. Chem. A* **3**, 11787–11795 (2015).
22. Peimyo, N. *et al.* Photocontrolled molecular structural transition and doping in graphene. *ACS Nano* **6**, 8878–8886 (2012).
23. Seo, S., Min, M., Lee, S. M. & Lee, H. Photo-switchable molecular monolayer anchored between highly transparent and flexible graphene electrodes. *Nat. Commun.* **4**, 1920 (2013).
24. Kim, M., Safron, N. S., Huang, C. H., Arnold, M. S. & Gopalan, P. Light-driven reversible modulation of doping in graphene. *Nano Lett.* **12**, 182–187 (2012).
25. Margapoti, E. *et al.* Emergence of photoswitchable states in a graphene–azobenzene–Au platform. *Nano Lett.* **14**, 6823–6827 (2014).
26. Mativetsky, J. M. *et al.* Azobenzenes as light-controlled molecular electronic switches in nanoscale metal-molecule-metal junctions. *J. Am. Chem. Soc.* **130**, 9192–9193 (2008).
27. Feng, Y. Y., Zhang, X. Q., Ding, X. S. & Feng, W. A light-driven reversible conductance switch based on a few-walled carbon nanotube/azobenzene hybrid linked by a flexible spacer. *Carbon* **48**, 3091–3096 (2010).
28. Rabe, J. P. & Buchholz, S. Commensurability and mobility in 2-dimensional molecular-patterns on graphite. *Science* **253**, 424–427 (1991).
29. Schlierf, A. *et al.* Nanoscale insight into the exfoliation mechanism of graphene with organic dyes: effect of charge, dipole and molecular structure. *Nanoscale* **5**, 4205–4216 (2013).
30. Yang, H. F. *et al.* Dielectric nanosheets made by liquid-phase exfoliation in water and their use in graphene-based electronics. *2D Mater.* **1**, 011012 (2014).
31. Griffiths, J. Photochemistry of azobenzene and its derivatives. *Chem. Soc. Rev.* **1**, 481–493 (1972).
32. Tamai, N. & Miyasaka, H. Ultrafast dynamics of photochromic systems. *Chem. Rev.* **100**, 1875–1890 (2000).
33. Bandara, H. M. D. & Burdette, S. C. Photoisomerization in different classes of azobenzene. *Chem. Soc. Rev.* **41**, 1809–1825 (2012).
34. Joseph, J. M., Destaillets, H., Hung, H. M. & Hoffmann, M. R. The sonochemical degradation of azobenzene and related azo dyes: rate enhancements via Fenton's reactions. *J. Phys. Chem. A* **104**, 301–307 (2000).
35. Turansky, R., Konopka, M., Doltsinis, N. L., Stich, I. & Marx, D. Switching of functionalized azobenzene suspended between gold tips by mechanochemical, photochemical, and opto-mechanical means. *Phys. Chem. Chem. Phys.* **12**, 13922–13932 (2010).
36. Surampudi, S. K., Patel, H. R., Nagarjuna, G. & Venkataraman, D. Mechano-isomerization of azobenzene. *Chem. Commun.* **49**, 7519–7521 (2013).
37. Shin, K. H. & Shin, E. J. Photoresponsive azobenzene-modified gold nanoparticle. *Bull. Korean Chem. Soc.* **29**, 1259–1262 (2008).
38. Ferrari, A. C. *et al.* Raman spectrum of graphene and graphene layers. *Phys. Rev. Lett.* **97**, 187401–187405 (2006).
39. Ferrari, A. C. & Robertson, J. Raman spectroscopy of amorphous, nanostructured, diamond-like carbon, and nanodiamond. *Philos. Trans. R. Soc. Lond. Ser. A* **362**, 2477–2512 (2004).
40. Ferrari, A. C. & Basko, D. M. Raman spectroscopy as a versatile tool for studying the properties of graphene. *Nat. Nanotechnol.* **8**, 235–246 (2013).
41. Tuinstra, F. & Koenig, J. L. Raman spectrum of graphite. *J. Chem. Phys.* **53**, 1126–1130 (1970).
42. Tan, P. H. *et al.* The shear mode of multilayer graphene. *Nat. Mater.* **11**, 294–300 (2012).
43. Lui, C. H. *et al.* Observation of layer-breathing mode vibrations in few-layer graphene through combination Raman scattering. *Nano Lett.* **12**, 5539–5544 (2012).
44. Ferrari, A. C. & Robertson, J. Resonant Raman spectroscopy of disordered, amorphous, and diamondlike carbon. *Phys. Rev. B* **64**, 075414–075426 (2001).
45. Ferrari, A. C. & Robertson, J. Interpretation of Raman spectra of disordered and amorphous carbon. *Phys. Rev. B* **61**, 14095–14107 (2000).
46. Thomsen, C. & Reich, S. Double resonant Raman scattering in graphite. *Phys. Rev. Lett.* **85**, 5214–5217 (2000).
47. Piscanec, S., Lazzeri, M., Mauri, F., Ferrari, A. C. & Robertson, J. Kohn anomalies and electron-phonon interactions in graphite. *Phys. Rev. Lett.* **93**, 185503 (2004).
48. Zheng, Y. B. *et al.* Surface-enhanced Raman spectroscopy to probe reversibly photoswitchable azobenzene in controlled nanoscale environments. *Nano Lett.* **11**, 3447–3452 (2011).
49. Chunder, A., Pal, T., Khondaker, S. I. & Zhai, L. Reduced graphene oxide/copper phthalocyanine composite and its optoelectrical properties. *J. Phys. Chem. C* **114**, 15129–15135 (2010).
50. Abraham, M. J. *et al.* GROMACS: high performance molecular simulations through multi-level parallelism from laptops to supercomputers. *SoftwareX* **1**, 19–25 (2015).
51. Schafer, L. V., Muller, E. M., Gaub, H. E. & Grubmuller, H. Elastic properties of photoswitchable azobenzene polymers from molecular dynamics simulations. *Angew. Chem. Int. Ed.* **46**, 2232–2237 (2007).
52. Pipolo, S. *et al.* First-principle-based MD description of azobenzene molecular rods. *Theor. Chem. Acc.* **131**, 1274–1287 (2012).
53. Ridley, J. & Zerner, M. An intermediate neglect of differential overlap technique for spectroscopy: pyrrole and the azines. *Theor. Chem. Acc.* **32**, 111–134 (1973).
54. Kondov, I., Cizek, M., Benesch, C., Wang, H. B. & Thoss, M. Quantum dynamics of photoinduced electron-transfer reactions in dye-semiconductor systems: first-principles description and application to coumarin 343-TiO₂. *J. Phys. Chem. C* **111**, 11970–11981 (2007).

Acknowledgements

We acknowledge funding from the European Commission through the Graphene Flagship (GA-604391), the Marie Curie project GREAT (PIEF-2011-GA-298246), the FP7-NMP-2012 project SACS (GA-310651), the Agence Nationale de la Recherche through the LabEx project Nanostructures in Interaction with their Environment (ANR-11-LABX-0058_NIE), the International Center for Frontier Research in Chemistry (icFRC), the Belgian National Fund for Scientific Research (FNRS), the FNRS/FRFC 'PHOTOGRAPH' PDR project, the Belgian Science Policy Office (IAP 7/05), the ERC synergy grant Hetero2D, ERC PoC HiGRAPHINK, and the Royal Society Wolfson Research Merit Award, EP/K01711X/1, EP/K017144/1 and EP/L016087/1. D.B. is a FNRS Research Director. M. Eredia, M. El Garah and A. Galanti are acknowledged for their assistance in X-ray photoelectron spectroscopy and high-performance liquid chromatography measurements.

Author contributions

P.S. and A.C. conceived the experiments and designed the study; M.D. and S.H. participated in the planning of the study and carried out the exfoliation (LPE) and characterization in solution (ultraviolet); M.D. performed the electrical characterization; S.H. and A.C. performed spectroscopic characterization; F.R. and S.H. performed the X-ray photoelectron spectroscopy experiments; M.D. and T.M. performed Kelvin probe measurements; M.B. and A.C.F. performed and analysed Raman experiments; S.O., A.M., R.L. and D.B. conducted theoretical studies; R.M. and V.M. analysed the samples with TEM; E.A.P. and L.D.C. performed and analysed X-ray diffraction experiments; all authors discussed results and contributed to the interpretation of data; D.B., A.C.F., A.C. and P.S. co-wrote the paper; all authors contributed to editing the manuscript.

Additional information

Supplementary Information accompanies this paper at <http://www.nature.com/naturecommunications>

Competing financial interests: The authors declare no competing financial interests.

Reprints and permission information is available online at <http://npg.nature.com/reprintsandpermissions/>

How to cite this article: Döbelin, M. *et al.* Light-enhanced liquid-phase exfoliation and current photoswitching in graphene–azobenzene composites. *Nat. Commun.* **7**:11090 doi: 10.1038/ncomms11090 (2016).



This work is licensed under a Creative Commons Attribution 4.0 International License. The images or other third party material in this article are included in the article's Creative Commons license, unless indicated otherwise in the credit line; if the material is not included under the Creative Commons license, users will need to obtain permission from the license holder to reproduce the material. To view a copy of this license, visit <http://creativecommons.org/licenses/by/4.0/>